EIS characteristics of antimony and its anodic oxide film in sulphuric acid solution

A S MOGODA[1],* and K M ZOHDY[2]

[1] Chemistry Department, Faculty of Science, Cairo University, Giza 12613, Egypt
[2] Higher Technology Institute, Tenth of Ramadan City 44629, Egypt
*Author for correspondence (awad.sadek@cu.edu.eg)

Abstract. The corrosion behaviour of antimony (Sb) and the stability of the anodic-generated coating on its surface were studied in a 4.97 M H_2SO_4 solution using cyclic voltammetry (CV), electrochemical impedance spectroscopy (EIS), potentiodynamic polarization, scanning electron microscopy (SEM) and atomic force microscopy (AFM). According to the CV data, the current plateau value increases as the scan rate increases, indicating that anodic layer development on the Sb surface occurs via a low-field migration mechanism. The EIS results confirmed that the pre-immersion oxide film and the anodic-produced layer on Sb are liable to dissolution in concentrated acid solution. The polarization results revealed that when the temperature rises, the rate of Sb corrosion in the acid solution increases. SEM and AFM surface investigation of the anodic layer generated on the antimony surface revealed that it is homogenous throughout its extension on the surface and lacks pores. For the corrosion of Sb in concentrated acid solution, the thermodynamic parameters E_a (activation energy), ΔH (enthalpy change) and ΔS (entropy change) were calculated.

Keywords. Antimony; cyclic voltammetry; EIS; SEM; polarization; AFM.

1. Introduction

In lead-acid battery grids, antimony is used as an alloying component [1–3]. It affects alloy casting and mechanical properties, as well as electrochemical reactions at the positive plate of the battery. Because of the lack of antimony, the battery's life is limited, especially after deep discharges. Antimony's electrochemical behaviour and the stability of its anodic oxide films in various aqueous and alcoholic-mixed solutions have previously been investigated [4–13]. The effects of antimony on the electrochemical processes of a lead electrode in sulphuric acid have been studied [14–19]. Depending on the electrode voltage, oxidation of Sb in the alloy resulted in a mixture of lead and antimony oxides of various compositions [15,16]. The goal of this study is to investigate the electrochemical behaviour of antimony in 4.97 M sulphuric acid. In addition, the surface properties of each air-formed film and anodic film, as well as their stabilities in concentrated sulphuric acid solution were compared. The experimental measurements of cyclic voltammetry (CV), potentiodynamic polarization, electrochemical impedance spectroscopy (EIS), scanning electron microscopy (SEM) and atomic force microscopy (AFM) have been accomplished in this study.

2. Experimental

2.1 *Materials*

The antimony rod (99.99%) was glued into a glass tube with an appropriate internal diameter using epoxy resin, leaving an antimony surface of 0.283 cm^2. The electrode was abraded down to 2000 grit with several grades of emery sheets, then wiped with a delicate cloth until it had a mirror-bright surface, then rinsed with double-distilled water before immersion in the electrolyte. Analytical grade chemical reagent and double-distilled water were used to make the sulphuric acid solution. Unless otherwise stated, all measurements were performed at 25°C in naturally aerated solutions.

2.2 *Electrochemical tests*

The electrochemical workstation 1M6e Zahner Elektrik (GmbH, Metechnik, Kronach, Germany) was used to perform open-circuit potential, CV, EIS and polarization experiments [20]. The input signal for impedance measurements was typically 10 mV peak to peak in the frequency domain 0.1–10^5 Hz [21–23]. The electrolytic cell was a three-electrode cell with an all-glass double jacket.

As an auxiliary electrode, a platinum sheet was employed. As a reference electrode, all potentials were measured and reported using an Ag/AgCl electrode.

2.3   *Surface characterization*

A scanning electron microscope (SEM, Quanta 250 FEG, FEI company, Netherlands) was used to examine the shape of the antimony surface after mechanically polishing and anodization in 4.97 M sulphuric acid solution. The topography of antimony's anodized surface was examined using an atomic force microscope (AFM) with a multifunctional probe head from Thermo-microscope (UK).

3.   Results and discussion

3.1   *Cyclic voltammetry*

Figure 1 shows cyclic voltammograms of an antimony electrode acquired with various scan rates in the potential range of –0.8 to +0.8 V in 4.97 M H_2SO_4 solution. The electrochemical reactions that occur in the anodic and cathodic portions of the antimony voltammetric have been examined previously [24–28], and we will focus primarily on the anodic portion here. The increase in current density through this section, as illustrated in figure 1, is caused by antimony active dissolution:

$$Sb + H_2O = SbO^+ + 2H^+ + 3e^- \tag{1}$$
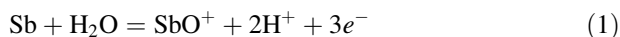
This reaction of active dissolution of Sb is controlled by the charge-transfer step and the diffusion of SbO^+ into the bulk solution. Accumulation of SbO^+ at the Sb surface at a high concentration leads to the production of a gel-like layer
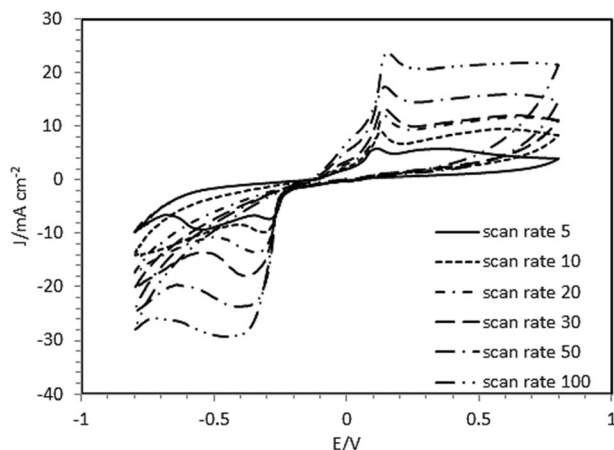
of $Sb(OH)SO_4$ and corresponds to the current maximum in the cyclic voltammogram:

$$SbO^+ + H^+ + SO_4^{(2-)} = Sb(OH)SO_4 \tag{2}$$

The dissolution of Sb is inhibited after the formation of the basic sulphate layer on its surface and causes a decrease in the current. As the potential increases, antimony dissolution occurs and when the rate of anodic production of antimony ions exceeds the rate of sulphate ions diffusing from the bulk of the solution to the Sb surface, antimony hydroxide sublayer forms:

$$Sb + 2H_2O = SbOOH + 3H^+ + 3e^- \tag{3}$$

A current plateau is formed where the growth and dissolution of the SbOOH sublayer occur at roughly the same rate. The height of the current plateau rises as the scan rate increases.

Figure 2 shows a linear relationship between the plateau current i_{pl} and the square root of scan rate $v^{1/2}$ for antimony. This result gives further support to the low-field migration mechanism for the oxide film growth on the Sb in the test solution [28–30]:

$$i = 2ABE, \tag{4}$$

where A and B are constants, and the product AB represents the anodic layer's ionic conductivity throughout growth. The following formula represents the field strength E:

$$E = (zF/V_m)(v/i_{pl}), \tag{5}$$

where z is the metal ion valency, V_m is the anodic layer phase's molar mass, and F is the Faraday constant. The following equation can be derived from equations (4) and (5):
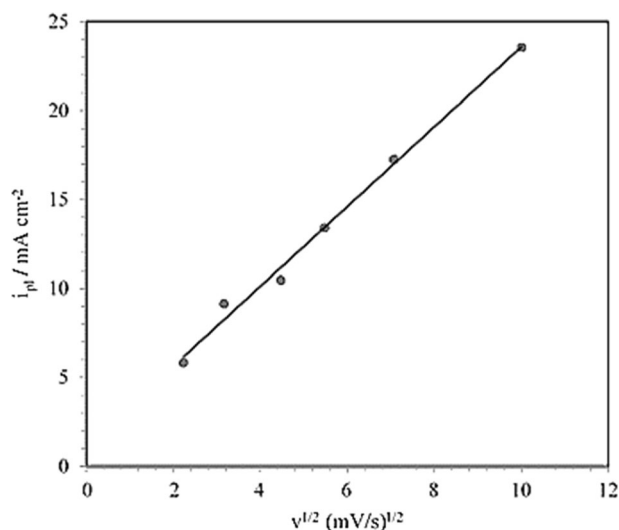
$$i_{pl} = (2ABzF/V_m)^{1/2}v^{1/2} \tag{6}$$

Figure 1.   Cyclic voltammograms of Sb in 4.97 M H_2SO_4 at different scan rates in mV s^{-1}.

Figure 2.   Dependence of plateau current on scan rate for Sb in 4.97 M H_2SO_4.
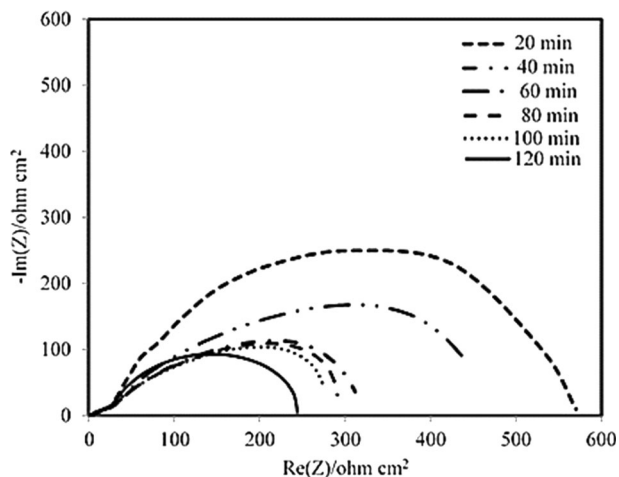
Figure 3. Nyquist plots of Sb in 4.97 M H$_2$SO$_4$ as a function of immersion time.
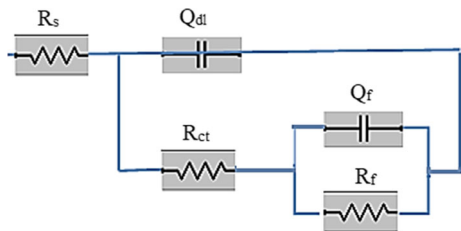

Figure 4. Equivalent circuit model for fitting the experimental EIS data.

Using the slope of the straight line in figure 2 and equation (6), we can calculate the ionic conductivity (*AB*) of the anodic layer on antimony, which was found to be 1.89×10^{-5} S cm^{-1}.

3.2 *EIS measurements*

3.2a *Mechanically polished antimony surface:* Antimony surface impedance spectra were measured in a 4.97 M H$_2$SO$_4$ solution at different immersion times. Nyquist plots of the experimental data are shown in figure 3. As seen in this figure, the diameter of the capacitive loop diminishes as antimony immersion time in the test solution rises. This suggests that the thickness of the air-formed passive film on the examined Sb surface decreases over time. Figure 4
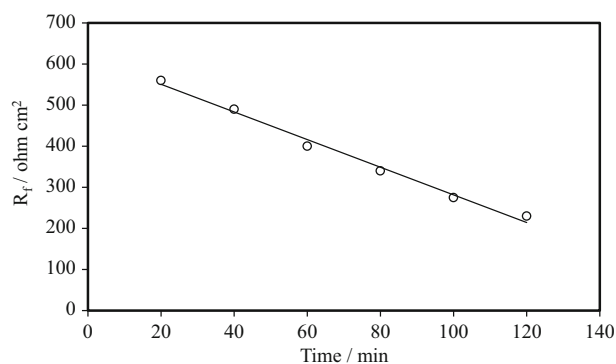

Figure 5. Variation of the air-formed film resistance, R_f, on Sb surface with immersion time in 4.97 M H$_2$SO$_4$.
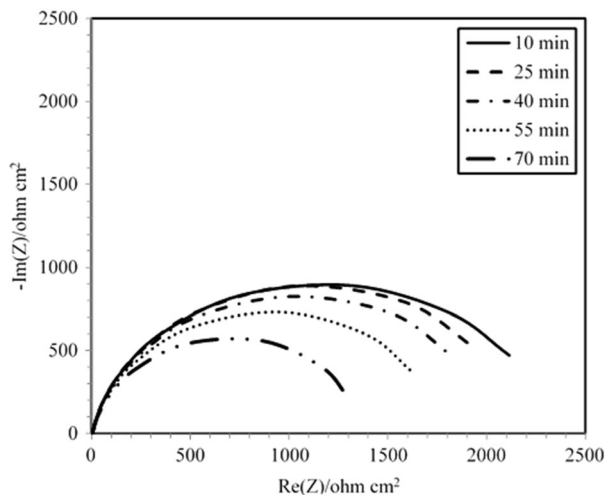

Figure 6. Nyquist plots of anodized antimony surface in 4.97 M H$_2$SO$_4$ as a function of immersion time.

depicts an equivalent electrical circuit for fitting the EIS spectra described here. The components in the circuit are as follows: R_s stands for solution resistance; R_{ct} is the charge transfer resistance; Q_{dl} denotes double-layer capacitance with constant phase angle element (CPE) behaviour; Q_f corresponds to capacitance due to the dielectric nature of the surface film; and R_f is the film resistance due to the surface film.

A similar equivalent electrical circuit was established for Ti-6Al-4V alloy in azide and halide anions [31], H$_3$PO$_4$ [32]

Table 1. Fitting parameters for the experimental impedance data of Sb in 4.97 M H$_2$SO$_4$ at different immersion times.

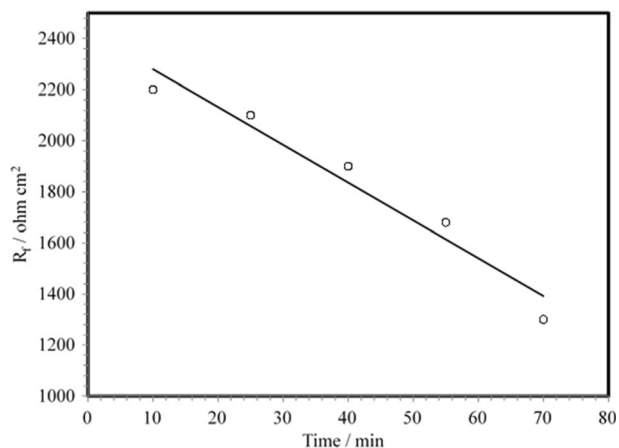| Time (min)	R_s (Ω cm^2)	R_{ct} (Ω cm^2)	$Q_{dl} \times 10^6$ (Ω^{-1} cm^{-2} s^n)	R_f (Ω cm^2)	$Q_f \times 10^6$ (Ω^{-1} cm^{-2} s^n)	α
20	2	33	113	570	3.79	0.86
40	2	31	124	489	3.86	0.83
60	2	29	135	398	3.90	0.85
80	2	28	139	341	3.97	0.82
100	2	27	142	276	4.12	0.84
120	2	25	147	234	4.88	0.87

Figure 7. Variation of the film resistance, R_f, of the anodized antimony surface with immersion time in 4.97 M H_2SO_4.

(a)

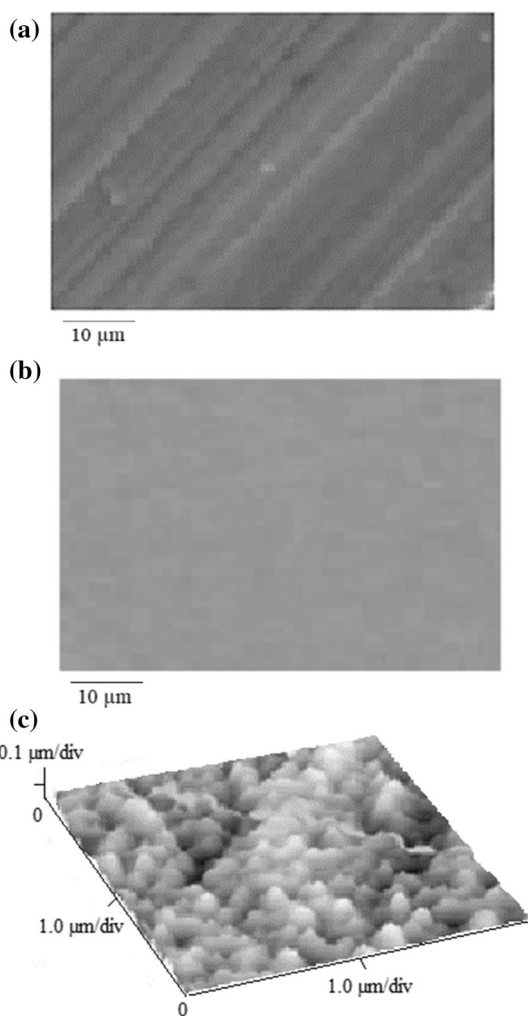**(b)**

(c)

Figure 8. SEM micrographs for (**a**) mechanically polished antimony surface, and (**b**) anodic film formed on antimony for 20 min at 0.5 V in 4.97 M H_2SO_4. (**c**) AFM image of sample **b**.

Figure 9. Potentiodynamic polarization of Sb in 4.97 M H_2SO_4 at different temperatures.

Table 2. Corrosion parameters of Sb in 4.97 M H_2SO_4 at different temperatures.

Temperature (°C)	E_{corr} (mV)	I_{corr} ($\mu A\ cm^{-2}$)	R_{corr} (mpy)
25	−102	107	128
35	−88	275	329
45	−87	367	440
55	−85	401	481
65	−81	598	715
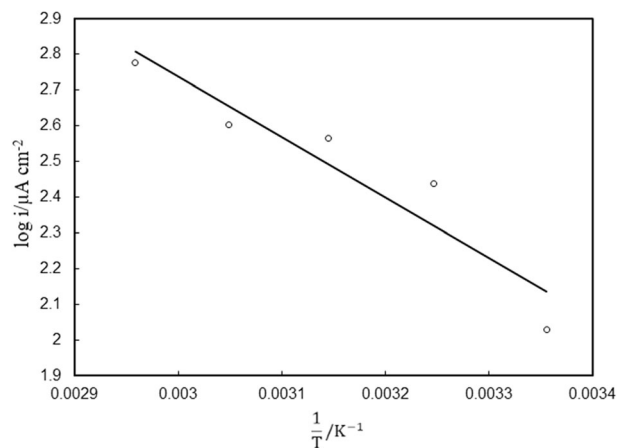
Figure 10. Arrhenius plots of the corrosion of Sb in 4.97 M H_2SO_4.

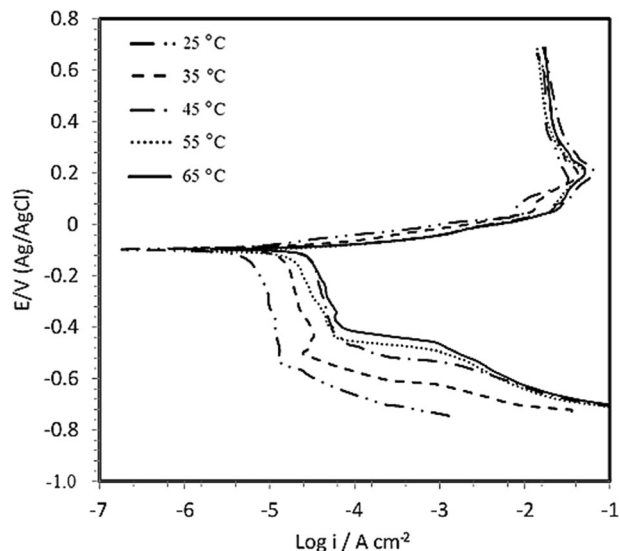and HBr [33]. Because there is a difference between real and pure capacitance, the EIS spectra can be simulated by substituting a CPE for the capacitance C. The impedance of the constant phase element is given by $Z = [Q(j\omega)^{\alpha}]^{-1}$, where Q is the frequency-independent real constant of CPE, ω is the angular frequency ($\omega = 2\pi f$), $j = \sqrt{-1}$, and the variable parameter α relates to surface roughness; it ranges from 1.0 for a flawlessly smooth surface with pure capacitive action to 0.5 for a porous surface [34,35]. The equivalent electrical circuit has two-time constants due to the surface film and

electrode surface. The fitted characteristic parameters for antimony EIS data in 4.97 M sulphuric acid are shown in table 1. The passive air-formed film resistance (R_f) decreases with increase in antimony immersion time in sulphuric acid, as seen in table 1. Figure 5 further demonstrates that R_f declines linearly with time at a rate of 3.35 ohm cm^2 min^{-1}.

3.2b *Anodized antimony surface:* Anodic polarization of the mechanically polished antimony surface in 4.97 M H$_2$SO$_4$ at a constant potential of 0.5 V was performed for 20 min. The antimony electrode was then withdrawn from the polarization cell and placed in a new H$_2$SO$_4$ solution of the same concentration, where EIS was monitored at different time intervals. Figure 6 illustrates that the diameter of the semicircle reduces as the immersion time for the anodic passive films on antimony in the concentrated acid solution rises. As shown in figure 7, the film resistance, R_f, of the anodic-generated film on antimony decreases with time in the acid solution at a rate of 14.67 ohm cm^2 min^{-1}. This is due to the dissolution of the anodic oxide film on antimony in the concentrated H$_2$SO$_4$. The resistance of the anodic film decreases at a higher rate (14.67 ohm cm^2 min^{-1}) than the resistance of the air-formed film (3.35 ohm cm^2 min^{-1}), showing that the anodic film has more defective properties than the air-formed film. This was previously seen for anodic film grown on titanium in NaF solution [36].

Figure 8a illustrates scratches and imperfections in the air-formed film on Sb, which are healed by forming a smooth anodic layer on the metal surface in the acid solution, as shown in figure 8b. Figure 8c shows an AFM image of the anodic layer on Sb, demonstrating that the film is homogeneous and pores-free.

3.3 *Polarization measurements*

The antimony electrode was immersed in the test solution until the steady-state open-circuit potential was reached before polarization measurements. Figure 9 depicts the potentiodynamic polarization curves of antimony in a 4.97 M H$_2$SO$_4$ solution at various temperatures. At different temperatures, table 2 illustrates the corrosion current density, I_{corr}, corrosion potential, E_{corr}, and antimony corrosion rate in mpy in 4.97 M sulphuric acid. The results in this table reveal that when the polarization temperature rises, the rate of antimony corrosion increases. The relationship between corrosion current density, I_{corr}, and temperature is governed by the Arrhenius equation [37]:

$$\frac{d \log I_{corr}}{d\left(\frac{1}{T}\right)} = -\frac{E_a}{2.303R}, \tag{7}$$

where E_a is the apparent activation energy of the corrosion process, R the gas constant (8.314 J mol^{-1} K^{-1}) and T is the

absolute temperature (K). Figure 10 shows the Arrhenius plot for antimony in 4.97 M H$_2$SO$_4$. The apparent activation energy of the corrosion process for antimony in the test solution is 32.3 kJ mol^{-1}. For antimony in 4.97 M H$_2$SO$_4$, the corrosion process parameters ΔH and ΔS are 29.7 kJ mol^{-1} and 93.1 kJ mol^{-1} K^{-1}, respectively.

4. Conclusions

The CV results showed that an anodic passive film on antimony grew in 4.97 M H$_2$SO$_4$, through the current plateau, which has an ionic conductivity of 1.89×10^{-5} S cm^{-1}. Both the air-formed and anodic films on antimony surfaces are vulnerable to dissolution in the acid medium, with the anodic film dissolving at a higher rate than the air-formed film (14.67 > 3.35 ohm cm^2 min^{-1}). This may be due to the fact that the anodic film that formed on the antimony surface has more defective characteristics than the air-generated film. The results of potentiodynamic polarization revealed that the rate of antimony corrosion increased as the temperature increased. SEM micrographs revealed that anodic polarization of the metal in 4.97 M H$_2$SO$_4$ repaired scratches and defects on the mechanically polished antimony surface. Furthermore, the AFM picture of the anodic-produced antimony film revealed that it was homogeneous and free of pores. E_a, ΔH and ΔS were calculated as thermodynamic parameters for the corrosion of Sb in concentrated acid solution.

References

[1] Brady G S 1971 *Handbook of materials* (New York: McGraw Hills Book Co.) p 64
[2] Take T and Akuto K 1988 *Electr. Commun.* **36** 5
[3] Mukerjee D and Guruviah S 1988 *Key Eng. Mater.* **20** 20
[4] El-Basiouny M S, Hefny M M and Mogoda A S 1984 *Annali di Chimica* **74** 729
[5] El-Basiouny M S, Hefny M M and Mogoda A S 1985 *Corrosion* **41** 611
[6] Hefny M M, Badawy W A, Mogoda A S and El-Basiouny M S 1985 *Electrochim. Acta* **30** 1017
[7] Badawy W A, Mogoda A S and Ibrahim M M 1988 *Electrochim. Acta* **33** 1367
[8] Gadallh A G, Salih S A, Hefny M M and Mogoda A S 1990 *Corrosion* **46** 214
[9] Mogoda A S, Badawy W A and Ibrahim M M 1995 *Bull. Electrochem.* **11** 281
[10] Mogoda A S, Badawy W A and Ibrahim M M 1995 Indian J. *Chem. Technol.* **2** 217
[11] Mogoda A S 2001 *Thin Solid Films* **394** 174
[12] Mogoda A S and Abd El-Haleem T M 2003 *Corrosion* **59** 3
[13] Mogoda A S and Abd El-Haleem T M 2003 *Thin Solid Films* **441** 6
[14] Laitinen T, Salmi K, Sundholm G, Morahovt B and Pavlovt D 1991 *Electrochim. Acta* **36** 605

[15] Pavlov D, Monahov B, Sundholm G and Laitinen T 1991 *J. Electroanal. Chem.* **305** 57

[16] Monahov B and Pavlov D 1994 *J. Electrochem. Soc.* **141** 2316

[17] Brinic S, Metikos-Hukovic M and Babic R 1995 *J. Power Sources* **55** 19

[18] Sun Q and Guo Y 2000 *J. Electroanal. Chem.* **493** 123

[19] Rocca E and Steinmetz J 2003 *J. Electroanal. Chem.* **543** 153

[20] El-Nowihy G H and El-Deab M S 2022 *J. Electrochem. Soc.* **169** 046508

[21] Mogoda A S and Farag A R 2022 *Silicon*. https://doi.org/10.1007/s12633-022-01861-x

[22] Mogoda A S, Zohdy K M and Aboutabl M A 2022 *Silicon* **14** 2573

[23] Mogoda A S and Zohdy K M 2022 *Int. J. Electrochem. Sci.* https://doi.org/10.20964/2022.01.23

[24] Bojinov M and Pavlov D 1991 *J. Electroanal. Chem.* **315** 201

[25] Pavlov D, Bojinov M, Laitinen T and Sundholm G 1991 *Electrochim. Acta* **36** 2081

[26] Pavlov D, Bojinov M, Laitinen T and Sundholm G 1991 *Electrochim. Acta* **36** 2087

[27] Metikos-Hukovic M, Babic R and Omanovic S 1994 *J. Electroanal. Chem.* **374** 199

[28] Metikos-Hukovic M, Babic R and Brinic S 2006 *J. Power Sources* **157** 563

[29] Williams D and Wright G A 1976 *Electrochim. Acta* **21** 1009

[30] Bojinov M, Kanazirski I and Girginov A 1995 *Electrochim. Acta* **40** 873

[31] El-Taib Heakal F, Ghoneim A A, Mogoda A S and Awad Kh A 2011 Corros. *Sci.* **53** 2728

[32] Ghoneim A A, Mogoda A S, Awad Kh A and El-Taib Heakal F 2012 *Int. J. Electrochem. Sci.* **7** 6539

[33] Ghoneim A A, El-Taib Heakal F, Mogoda A S and Awad Kh A 2010 *Surf. Interface Anal.* **42** 1695

[34] Juttner K 1990 *Electrochim. Acta* **35** 1501

[35] Rammelt U and Reinhard G 1990 *Electrochim. Acta* **35** 1045

[36] Mogoda A S and Zohdy K M 2020 *Int. J. Electrochem. Sci.* **15** 8070

[37] Atkins P W 1998 *Physical Chemistry* (Oxford University Press) p 864